Optimal Surface Salinity Perturbations Influencing the Thermohaline Circulation

FLORIAN SÉVELLEC, MAHDI BEN JELLOUL, AND THIERRY HUCK

Laboratoire de Physique des Océans, Université de Bretagne Occidentale, Brest, France

ABSTRACT

Optimal surface salinity perturbations influencing the meridional overturning circulation maximum are exhibited and interpreted on a stable steady state of a 2D latitude–depth ocean thermohaline circulation model. Despite the stability of the steady state, the nonnormality of the dynamics is able to create some transient growth and variability through stimulation by optimal perturbations. Two different measures are compared to obtain the optimum—one associated with the departure from steady state in terms of density, and the other with the overturning circulation intensity. It is found that such optimal analysis is measure dependent; hence, the latter measure is chosen for studying the following physical mechanisms. The response to the optimal initial sea surface salinity perturbation involves a transient growth mechanism leading to a maximum modification of the circulation intensity after 67 yr; the amplification is linked to the most weakly damped linear eigenmode, oscillating on a 150-yr period. Optimal constant surface salinity flux perturbations are also obtained, and confirm that a decrease in the freshwater flux amplitude enhances the circulation intensity. At last, looking for the optimal stochastic surface salinity flux perturbation, it is established that the variance of the circulation intensity is controlled by the weakly damped 150-yr oscillation. Two approaches are tested to consider extending such studies in more realistic 3D models. Explicit solutions (versus eigenvalue problems) are found for the overturning circulation measure (except for the stochastic optimal); a truncation method on a few leading eigenmodes usually provides the optimal perturbations for analyses on long time scales.

---

1. Introduction

One of the expected consequences of global warming is the modification of the water cycle, one of the main forcing mechanisms of the ocean thermohaline circulation. In actuality, freshwater fluxes have a local influence on the surface salinity, and thus on the ocean dynamics. Josey and Marsh (2005) show that sea surface salinity has been modified since the mid-1970s because of increased precipitation in the North Atlantic Ocean subpolar gyre. Modification of ocean salinity in the recent decades is also found deeper in the North Atlantic (Curry et al. 2003; Curry and Mauritzen 2005). These studies point out that the water cycle is the least-understood part of the climate system because evaporation and precipitation over the ocean have large measurement uncertainties. As the slow component of the climate system, the ocean, and more particularly the thermohaline circulation, is the best candidate to produce low-frequency variability. Given these considerations, in this study we will focus on the impact of freshwater flux on the thermohaline circulation.

In the ocean, two paradigms coexist to explain the observed variability: the variability could be either endogenous or exogenous. For the first paradigm, the variability is due to internal modes, such as millennial [e.g., Colin de Verdière et al. (2006): relaxation oscillation] or centennial [e.g., Sévellec et al. (2006): nonlinear saturation of a linear growing mode] oscillation; this theory relies intrinsically on nonlinear effects. The second paradigm is based on the hypothesis of a stable steady state of the ocean circulation and the presence of an external stimulation needed to sustain the variability, for example, oscillations sustained by stochastic freshwater forcing on centennial (Mysak et al. 1993; Mikolajewicz and Maier-Reimer 1990) and multidecadal (Griffies and Tziperman 1995) time scales. Because of the nonnormal nature of the ocean dynamics, some perturbations can produce dramatic variability

Corresponding author address: Florian Sévellec, Laboratoire d'Océanographie et du Climat, Expérimentation et Approches Numériques (UMR 7159 CNRS IRD UPMC MNHN), Institut Pierre Simon Laplace, case 100, 4 place Jussieu, CEDEX 05, 75252 Brest, France.
E-mail: florian.sevellec@locean-ipsl.upmc.fr

around a steady state even though it is stable. Transient amplification of initial perturbations has been analyzed in both the atmospheric (Farrell and Ioannou 1996) and oceanic (Farrell and Moore 1992; Moore and Farrell 1993; Moore et al. 2002) contexts, and more recently for coupled El Niño variability (Moore et al. 2003). Our study belongs to this last paradigm, because we will study the variability of the ocean circulation perturbed by freshwater flux.

Some previous work has been done on the variability of the thermohaline circulation in accordance with this second paradigm. Lohmann and Schneider (1999) investigated optimal initial and stochastic perturbations in Stommel's (1961) two-box model, with applications to initial error growth and predictability. Sirkes and Tziperman (2001) used the adjoint of a 3D primitive-equation model to establish the sensitivity of heat transport at 24°N, and found an oscillatory mode of centennial time scale with basically the same properties and mechanism as that of the interdecadal oscillation previously studied in box models (Tziperman et al. 1994; Griffies and Tziperman 1995). In a three-box model, Tziperman and Ioannou (2002) have analyzed the optimal finite-time growth of a measure defined as the square of the circulation intensity. The mechanism, resulting from the mixed boundary conditions, corresponds to a rapid decay of the temperature of the anomaly, initially balanced in terms of density, which induces a salinity-driven circulation anomaly in a finite time before the slower decay of the salinity anomaly. Looking for the optimal stochastic perturbation, these authors found that no peak appears in the frequency range of their analysis despite the existence of a linear damped oscillatory mode. In Stommel's (1961) two-box model of the thermohaline circulation, Mu et al. (2004) search the optimal initial condition within a nonlinear approach called conditional nonlinear optimal perturbation (CNOP); the authors show the limit of the linear approximation, and highlight the asymmetry of the advection term in the nonlinear equations. These conclusions are extended within a coupled ocean–atmosphere box model (Sun et al. 2005); furthermore, their results suggest that a linear approach is valid for studying weak overturning variations of the present thermohaline circulation. More recently, Zanna and Tziperman (2005) studied the optimal perturbation and analyzed its transient growth in a simple coupled model (a latitude–depth ocean model with two levels on the vertical and a one-layer atmosphere); they find the optimal initial perturbation maximizing some kind of spatial variance transport after 40 yr. Their amplification mechanism involves the growth of both temperature and salinity

perturbations resulting from the advection by the anomaly circulation.

As a follow-up to these works, we will address successively the response of our nonnormal dynamical system to impulsive and then to continuous excitations (Farrell and Ioannou 1996). Hence, we look for the optimal pattern of initial surface salinity perturbation, constant freshwater flux, and stochastic freshwater flux, impacting the thermohaline circulation, within a linear framework. The evaluation of a perturbation impact requires the definition of a measure of the thermohaline circulation. In contrast with previous works, two different measures will be compared here—one taking into account all the prognostic-state variables of the model (temperature and salinity, in terms of density), and a second (more physical and more intuitively analyzed) related to the overturning circulation. Solving for these optimal perturbations leads to maximization problems whose solutions are exhibited either implicitly through an eigenvalue problem for the first measure, or explicitly for the second. As a first step, numerical applications are computed here in a 2D latitude–depth ocean model to represent the North Atlantic thermohaline circulation. As compared with previous work in box geometry, this model provides significant improvements on the structure of the mean overturning, and the periods of the internal modes are much more robust. Optimal perturbations show a predictable large-scale structure that will be discussed in terms of linear and adjoint eigenmodes. The ocean model response to these perturbations will be interpreted in terms of physical processes. For instance, the transient growth mechanism is related here to the positive salinity feedback on the overturning, which is not obvious in the box model results (Tziperman and Ioannou 2002); furthermore, under optimal stochastic forcing, the period of the least-damped eigenmode dominates the power spectrum density, whereas it does not appear in the box model (Tziperman and Ioannou 2002). Optimal perturbations are also computed through a truncation of the linear and adjoint models to an incomplete sum of their leading eigenmodes. This method is successful and allows for better interpretation of the optimal perturbations, but especially the consideration of applications in more realistic models.

The paper is organized as follows. The equations and parameters of the model are described in section 2. The reference stable steady state and its linear stability analysis are discussed in section 3. The description of the two measures, the possible perturbation constraints, and the analytical method of maximization are made explicit in section 4. The paper proceeds following the three questions: What is the optimal initial perturbation

of the surface salinity that induces the largest variation of the thermohaline circulation (section 5)? What is the optimal constant perturbation of the surface salinity flux that induces the largest variation of the thermohaline circulation (section 6)? What is the optimal stochastic perturbation of the surface salinity flux that induces the largest variation of the thermohaline circulation (section 7)? Conclusions are drawn in section 8.

2. The ocean model

The latitude–depth 2D model (Sévellec et al. 2006) is based on the 3D planetary geostrophic equations in Cartesian coordinates, where zonal averaging requires some dynamical approximations (Marotzke et al. 1988; Wright and Stocker 1991; Wright et al. 1995, 1998; here we use linear friction, leading to

$$-\rho_0^{-1}\partial_y P - \varepsilon v = 0, \qquad (1a)$$

$$-\partial_z P - \rho g = 0, \quad \text{and} \qquad (1b)$$

$$\partial_y v + \partial_z w = 0, \qquad (1c)$$

where y is latitude, z is the vertical coordinate, P is the pressure, ρ (ρ_0) is the (reference) density, (v, w) is the velocity, and g is the gravity acceleration. The choice of the linear friction coefficient $\varepsilon = 1.45 \times 10^{-4}$ s^{-1} leads to a realistic overturning $\simeq 15$ Sv (1 Sv $\equiv 10^6$ m^3 s^{-1}) for a typical North Atlantic thermohaline stratification. This solution corresponds to a very frictional system where the meridional momentum dynamical balance is between the pressure gradient and the linear friction, as in Stommel's (1961) box model.

A linearized equation of state for the seawater is used:

$$\rho = \rho_0[1 - \alpha(T - T_0) + \beta(S - S_0)], \qquad (2)$$

where α is the thermal expansion coefficient, T (T_0) is the (reference) temperature, β is the haline contraction coefficient, and S (S_0) is the (reference) salinity.

Only the thermodynamic equations are prognostic:

$$\partial_t T = -J(\psi, T) + K_H\partial_y^2 T + K_V\partial_z^2 T + \mathcal{F}_T \quad \text{and} \quad (3a)$$

$$\partial_t S = -J(\psi, S) + K_H\partial_y^2 S + K_V\partial_z^2 S + \mathcal{F}_S, \qquad (3b)$$

where J is the Jacobian operator, ψ is the overturning streamfunction defined as $w = \partial_y\psi$ and $v = -\partial_z\psi$, and $K_H(K_V)$ is the horizontal (vertical) eddy diffusivity. Convection is not explicitly represented, particularly to simplify the linearization. Zhang et al. (1992), as well as Marotzke and Scott (1999), have suggested that convective adjustment does not matter as crucially for a

TABLE 1. Parameters used for the 2D model time integrations, with their values and definitions.

n_y	28	No. of grid points in latitude
n_z	15	No. of grid points in the vertical
H	4500 m	Ocean uniform depth
W	5120 km	Zonal basin extent
y_0	10°N	Southern boundary position
y_1	60°N	Northern boundary position
K_H	10^3 m^2 s^{-1}	Horizontal tracer diffusion
K_V	10^{-4} m^2 s^{-1}	Vertical tracer diffusion
g	9.8 m s^{-2}	Gravitational acceleration
ρ_0	1027 kg m^{-3}	Reference density
α	2.2×10^{-4} K^{-1}	Thermal expansion coefficient
β	7.7×10^{-4} psu^{-1}	Haline contraction coefficient
τ_T	66 days	Temperature-restoring time
F_0	75 cm yr^{-1}	Freshwater flux intensity
T_0^*	13.5°C	Restoring temperature amplitude
ε	1.45×10^{-4} s^{-1}	Linear friction coefficient

realistic thermohaline structure in 2D as in 3D because its effect remains efficiently represented through downwelling. Surface boundary conditions for temperature and salinity will differ ("mixed boundary conditions") to take into account the different feedbacks of sea surface temperature (SST) and salinity (SSS), respectively, on surface heat and freshwater flux. The surface forcing is then expressed as

$$\mathcal{F}_T = \tau_T^{-1}[T^*(y) - \text{SST}(y)] \quad \text{and} \qquad (4a)$$

$$\mathcal{F}_S = \frac{S_0}{h}\text{FW} \qquad (4b)$$

in the uppermost model level of thickness $h = 50$ m; the restoring surface temperature and the freshwater flux are

$$T^*(y) = T_0^*\{1 + \cos[\pi(y - y_0)/(y_1 - y_0)]\}, \quad \text{and}$$
$$(5a)$$

$$\text{FW}(y) = -F_0 \sin[2\pi(y - y_0)/(y_1 - y_0)]. \qquad (5b)$$

These equations are solved by using a finite difference formulation (see Table 1 for the model parameter values) on a uniform latitudinal grid but a nonuniform vertical grid (15 levels of thickness varying from 50 m at the surface to 550 m at the bottom). No-normal-flow conditions are used on the boundaries, resulting in a zero streamfunction, and zero flux conditions are applied to temperature and salinity except at the surface.

3. Linear stability analysis

We first describe the steady state used in all the following study and the results from its linear stability
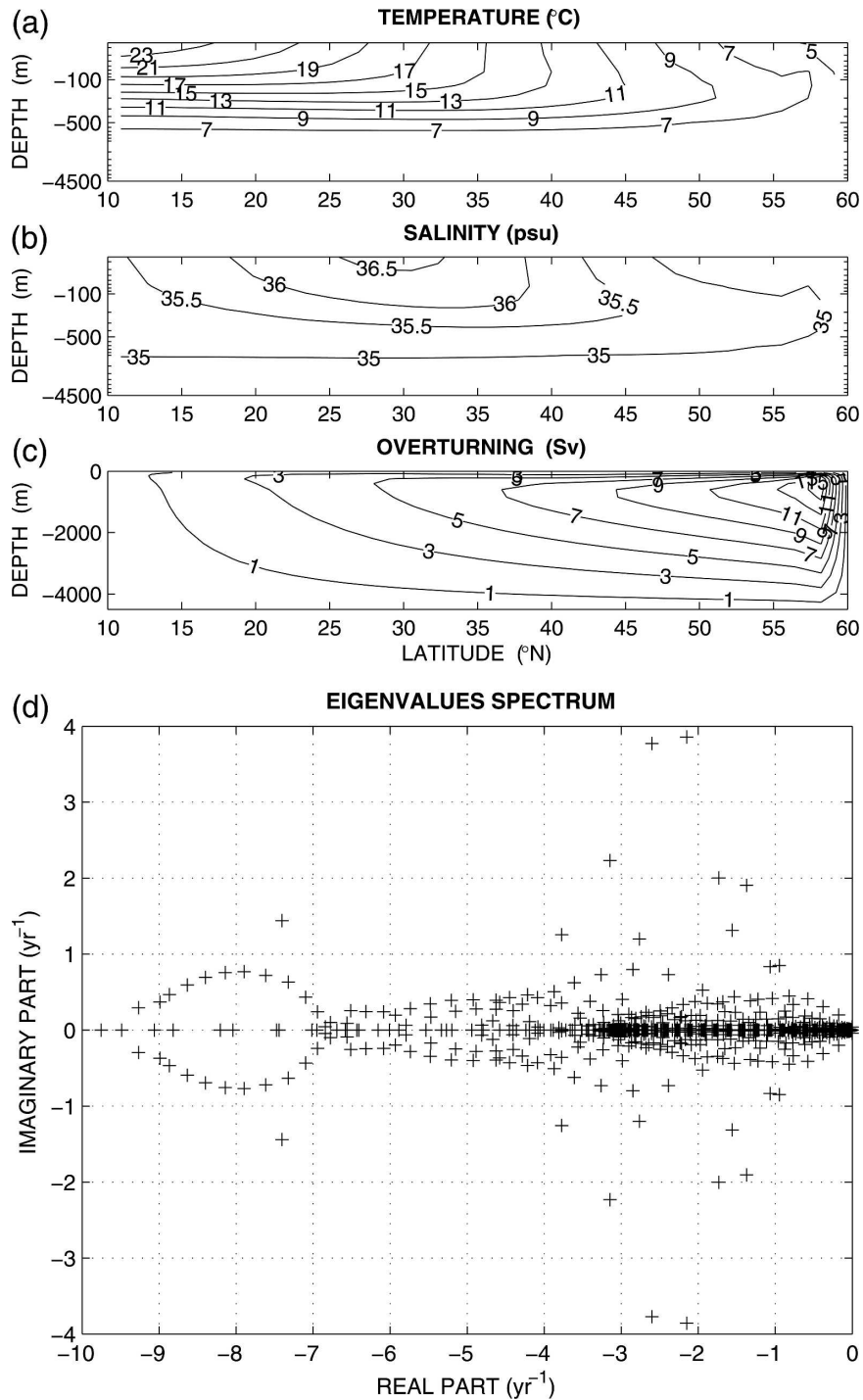
FIG. 1. Stable steady state of the 2D model: (a) temperature, (b) salinity (both represented with a logarithmic depth axis), and (c) meridional overturning streamfunction (contour intervals are respectively 2°C, 0.5 psu, and 2 Sv). (d) The eigenvalues spectrum from the linear stability analysis.

analysis. Figures 1a–c show the temperature, salinity, and meridional overturning field in the steady state obtained after a 10 000 yr-long time integration of the nonlinear 2D model.

The principle of linear stability analysis is to examine the evolution of a small perturbation near a steady state. The prognostic equations of our model (3) can be written as a general dynamical system,

$$d_t|\mathbf{U}\rangle = \mathcal{N}(|\mathbf{U}\rangle), \qquad (6)$$

where $\mathcal{N}$ is a nonlinear operator and $|\mathbf{U}\rangle$ is the state vector consisting of temperature and salinity at every grid points, written as a ket; the associated bra $\langle\mathbf{U}|$ is defined through the Euclidian scalar product $\langle\mathbf{U}|\mathbf{U}\rangle$. Let $|\overline{\mathbf{U}}\rangle$ be a steady state, that is, $\mathcal{N}(|\overline{\mathbf{U}}\rangle) = 0$; the evolution of the perturbation $|\mathbf{u}\rangle = |\mathbf{U}\rangle - |\overline{\mathbf{U}}\rangle$ by the linearized dynamics is

$$d_t|\mathbf{u}\rangle = \mathbf{A}|\mathbf{u}\rangle, \quad \text{where} \quad \mathbf{A} = \left.\frac{\partial\mathcal{N}}{\partial|\mathbf{U}\rangle}\right|_{|\overline{\mathbf{U}}\rangle}, \qquad (7)$$

where the Jacobian operator $\mathbf{A}$ depends only on the steady state $|\overline{\mathbf{U}}\rangle$ (autonomous system). We can then integrate to get the perturbation time evolution,

$$|\mathbf{u}(t)\rangle = \exp(\mathbf{A}t)|\mathbf{u}(0)\rangle = \mathbf{M}(t)|\mathbf{u}(0)\rangle, \qquad (8)$$

where $\mathbf{M}(t)$ is called the propagator.

The Jacobian operator is calculated by linearization of the full model equations, both analytically and numerically (Huck and Vallis 2001) with identical results. Once the Jacobian operator is computed for our steady state, an eigenanalysis is performed; the spectrum of the eigenvalues and the least-damped mode is represented respectively in Figs. 1d and 2. All of the eigenvalues have a negative real part, in agreement with a stable steady state obtained through time integration. The presence of complex eigenvalues reveals the existence of internal oscillatory modes. Actually, the least-damped eigenmode corresponds to a weakly damped 150-yr oscillation that has been largely studied in Sévellec et al. (2006). For stronger freshwater forcing, the steady state becomes unstable and oscillations appear with a slightly longer period. Sévellec et al. (2006) showed that the period is mainly controlled by the mean flow advection of salt perturbation and the growth is due to the competition between diffusion and salinity perturbation reinforcement at the surface. The sensitivity of this eigenmode characteristic has been tested with various horizontal and vertical resolutions (respectively, 14 and 42 points, with 10 and 20 levels). Its period varies between 140 and 176 yr with a similar thermohaline structure, whereas the growth rate increases regularly with increasing resolution as the Hopf bifurcation threshold slightly changes.

To interpret the generalized stability theory, we perform an eigenanalysis of the adjoint (linear transposed) model. As the theory predicts, the spectrum is the same but the eigenvectors are different because of the nonnormality of our linear operator ($\mathbf{A}\mathbf{A}^\dagger - \mathbf{A}^\dagger\mathbf{A} \neq 0$, where † denotes the Hermitian operator). The least-damped eigenvectors are represented in Figs. 2g–l. The eigenvectors of $\mathbf{A}^\dagger$ are defined as the biorthogonal vectors of the eigenvectors of $\mathbf{A}$. They have two main properties—their eigenvalues are complex conjugates and their contravariant projections are maximum.

4. Maximization method

We now present the method we will use to obtain the different optimal profiles of sea surface salinity, surface salinity flux, or stochastic salinity flux, maximizing either the meridional overturning circulation intensity or a thermohaline density norm.

We are looking for a vector that under some constraints maximizes some scalar quantity related to the system state. Let $|\mathbf{u}\rangle$ be the state vector; $G(|\mathbf{u}\rangle)$ is the scalar function to be maximized under the n constraints $C_i(|\mathbf{u}\rangle) = 0$ for $i = 1, \ldots, n$. It is then convenient to introduce the Lagrangian

$$\mathcal{L}(|\mathbf{u}\rangle, \gamma_i) = G(|\mathbf{u}\rangle) - \sum_{i=0}^{n}\gamma_i C_i(|\mathbf{u}\rangle), \qquad (9)$$

where the γs are the Lagrangian parameters associated with the constraints.

The state $|\mathbf{u}\rangle$ that maximizes G under these constraints verifies

$$d\mathcal{L}(|\mathbf{u}\rangle, \gamma_i) = \frac{\partial\mathcal{L}}{\partial|\mathbf{u}\rangle}d|\mathbf{u}\rangle - \sum_{i=0}^{n}\frac{\partial\mathcal{L}}{\partial\gamma_i}d\gamma_i = 0, \qquad (10)$$

that is,

$$\frac{d\mathcal{L}}{d|\mathbf{u}\rangle} = \frac{dG(|\mathbf{u}\rangle)}{d|\mathbf{u}\rangle} - \sum_{i=0}^{n}\gamma_i\frac{dC_i(|\mathbf{u}\rangle)}{d|\mathbf{u}\rangle} = 0 \quad \text{and} \qquad (11a)$$

$$\frac{d\mathcal{L}}{d\gamma_i} = -C_i(|\mathbf{u}\rangle) = 0, \quad \text{where} \quad \forall i = 1, \ldots, n. \qquad (11b)$$

Solving this maximization problem depends on the kind of scalar function that is being maximized. In the following we choose two scalar functions that are appropriate for the physical problem we want to address: a linear function, approximating the meridional overturning circulation intensity that we will write as $\langle F|\mathbf{u}\rangle$; and a quadratic function, measuring the thermohaline density norm of the perturbation state $\langle\mathbf{u}|\mathbf{S}|\mathbf{u}\rangle$, where $\mathbf{S}$ is a diagonal weight matrix that enforces homogeneity. This norm is such that all coordinates of the state perturbation are summed after being rescaled in terms of their squared density and their respective volume (v_i): $\langle\mathbf{u}|\mathbf{S}|\mathbf{u}\rangle = \Sigma_i[(\alpha^2 T_i^2 + \beta^2 S_i^2)v_i]/(\Sigma_i v_i)$; in other words, it measures the departure from steady-state tempera-
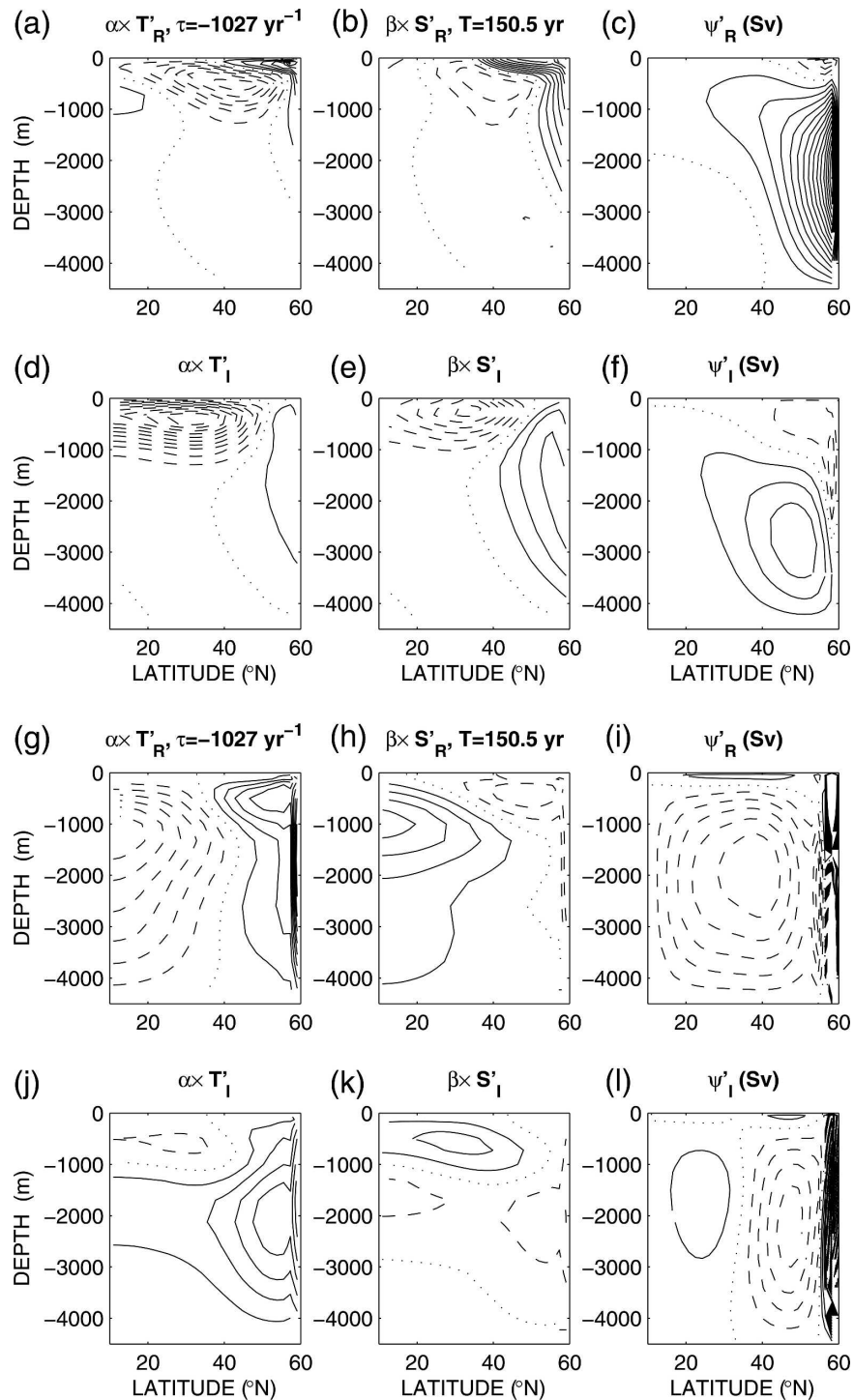
FIG. 2. The least-damped couple of eigenmodes of the (a)–(f) tangent linear and (g)–(l) adjoint operators (their biorthogonal vectors): (a), (d), (g), (j) temperature and (b), (e), (h), (k) salinity in terms of density and (c), (f), (i), (l) associated streamfunction. Their common eigenvalues are complex conjugates and the mode represents a 150-yr-period oscillation damped on a 1027-yr time scale, evolving from the real part to the imaginary part, and to their opposites. The solid, dashed, and dotted lines, respectively, correspond to positive, negative, and zero anomalies; contour intervals are (a)–(f) 2.5×10^{-6} for temperature and salinity, 0.25 Sv for streamfunction, and (g)–(l) 5×10^{-7} for temperature, 2×10^{-5} for salinity, and 2 Sv for streamfunction.

ture and salinity in terms of density. Because the over-turning intensity is the streamfunction maximum that is not a differentiable function of the system state, the maximum is estimated as the mean value of the closest nine grid points to the real maximum value (actually, only six of them are nonzero because the maximum of the overturning streamfunction is very close to the northern boundary, and it is zero on those grid points to respect the no-normal-flux boundary conditions). Writing successively in matrix form (1b), (1a), ψ as a function of v, and ψ_{max} as a function of ψ: $|P\rangle = \mathbf{F}_1|\mathbf{u}\rangle$, $|v\rangle = \mathbf{F}_2|P\rangle$, $|\psi\rangle = \mathbf{F}_3|v\rangle$, $\psi_{max} = \langle F_4|\psi\rangle$, we obtain ψ_{max} as a linear function of $|\mathbf{u}\rangle$, that is, $\psi_{max} = \langle F|\mathbf{u}\rangle$ with $\langle F| = \langle F_4|\mathbf{F}_3\mathbf{F}_2\mathbf{F}_1$. The accuracy of the six-point approximation is tested on the steady state and the streamfunction maximum is then underestimated by an amount that does not exceed 15%.

Let us now define the constraints we use. First, we only allow perturbations of surface salinity satisfying salinity conservation. This is coherent with the salt conservation equation of the model; otherwise, the trend in the total salt may induce a perpetual drift. This constraint is made implicit by using the projection $|\mathbf{u}\rangle = \mathbf{P}|\mathbf{u}'\rangle$, where $|\mathbf{u}'\rangle$ is a vector of the subspace of surface salinity–conserving salt (dimension $n_y - 1$), and $\mathbf{P}$ is the associated projection operator (dimension $2n_y n_z, n_y - 1$). For instance, $\mathbf{P}$ is zero everywhere except for one 1 on each line of ($n_y - 1$) surface salinity points for the corresponding surface salinity value, and a full line of (-1) on the remaining surface salinity point. Second, because we deal with a linear problem, all of the optima are computed up to a multiplicative factor. To remove this degeneracy we seek normed perturbations using the weight matrix $\langle \mathbf{u}|\mathbf{S}|\mathbf{u}\rangle = 1$. The associated constraint is explicitly stated and an associated Lagrange parameter is introduced.

Because the same kind of algebra is used for different investigations, the recurrent Lagrangian is written in the following form: $\mathcal{L}_x^y$, $x \in \{ini, cst, sto\}$, $y \in \{N, C\}$, where the subscript indicates the type of the optimal being computed (optimal initial surface salinity perturbation, optimal constant and stochastic surface salinity flux) and the superscript is the quantity being maximized (N for the thermohaline density norm and C for the circulation intensity).

5. Optimal initial surface salinity perturbation

In this section, we address our first question: what is the optimal initial perturbation of the SSS that induces the largest variation of the thermohaline circulation? This variation is measured successively in two different manners, through the quadratic thermohaline density

norm and the meridional overturning circulation (MOC) intensity.

We first seek the initial SSS perturbation inducing the maximum change within the finite time scale τ in terms of the thermohaline density norm. The Lagrangian is

$$\mathcal{L}_{ini}^N = \langle \mathbf{u}(\tau)|\mathbf{S}|\mathbf{u}(\tau)\rangle - \gamma[\langle \mathbf{u}(0)|\mathbf{S}|\mathbf{u}(0)\rangle - 1], \quad (12)$$

where γ is the Lagrange parameter associated with the norm constraint. The initial surface salinity perturbation vector $[|\mathbf{u}(0)\rangle = \mathbf{P}|\mathbf{u}_0'\rangle]$ must satisfy the following:

$$d\mathcal{L}_{ini}^N = d\langle \mathbf{u}_0'|\mathbf{P}^\dagger \mathbf{M}^\dagger(\tau)\mathbf{S}\mathbf{M}(\tau)\mathbf{P}|\mathbf{u}_0'\rangle - \gamma d\langle \mathbf{u}_0'|\mathbf{P}^\dagger \mathbf{S}\mathbf{P}|\mathbf{u}_0'\rangle = 0, \quad (13)$$

which can be rewritten as an eigenvalue problem,

$$\mathbf{N}^{-1}\mathbf{H}_{ini}^N(\tau)|\mathbf{u}_0'\rangle = \gamma|\mathbf{u}_0'\rangle, \quad (14)$$

where $\quad \mathbf{N} = \mathbf{P}^\dagger \mathbf{S}\mathbf{P} \quad$ and $\quad \mathbf{H}_{ini}^N(\tau) = \mathbf{P}^\dagger \mathbf{M}^\dagger(\tau)\mathbf{S}\mathbf{M}(\tau)\mathbf{P}$. (15)

Note that although $\mathbf{P}$ is rectangular, $\mathbf{S}$ defines a scalar product; hence, $\mathbf{N}$ is Hermitian and has an inverse. The optimal solution, that is, the surface salinity perturbation inducing the largest finite-time growth of the perturbation density norm, corresponds to the eigenmode whose associated eigenvalue has the largest real part. The optima were computed in our 2D model for different growth times τ, and a local maximum growth appears for $\tau = 96$ yr (Fig. 3); its linear time integration reveals nonnormal decay. The initial SSS profile corresponding to this maximum growth and its associated perturbation of temperature, salinity, and overturning circulation after 96 yr are shown in Fig. 3.

We now seek the initial SSS perturbation inducing the largest finite-time growth of the overturning circulation intensity. The Lagrangian function is now expressed as

$$\mathcal{L}_{ini}^C(\tau) = \langle F|\mathbf{u}(\tau)\rangle - \gamma[\langle \mathbf{u}(0)|\mathbf{S}|\mathbf{u}(0)\rangle - 1]. \quad (16)$$

The optimal SSS perturbation vector must satisfy

$$d\mathcal{L}_{ini}^C(\tau) = d\langle F|\mathbf{M}(\tau)\mathbf{P}|\mathbf{u}_0'\rangle - \gamma d\langle \mathbf{u}_0'|\mathbf{P}^\dagger \mathbf{S}\mathbf{P}|\mathbf{u}_0'\rangle = 0, \quad (17)$$
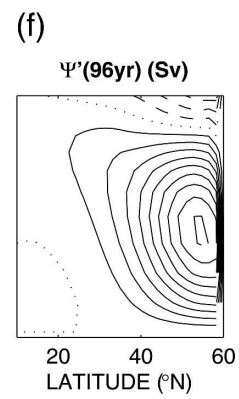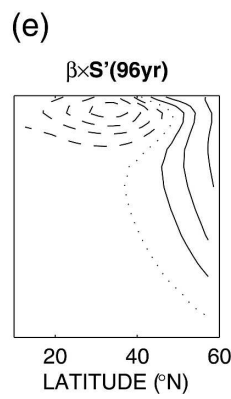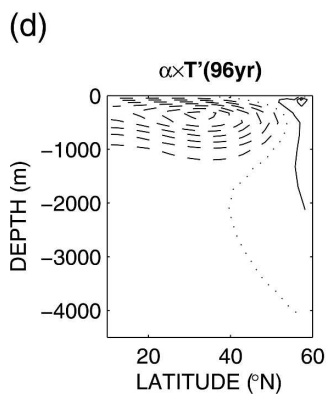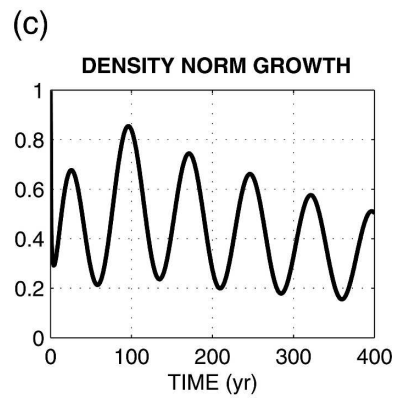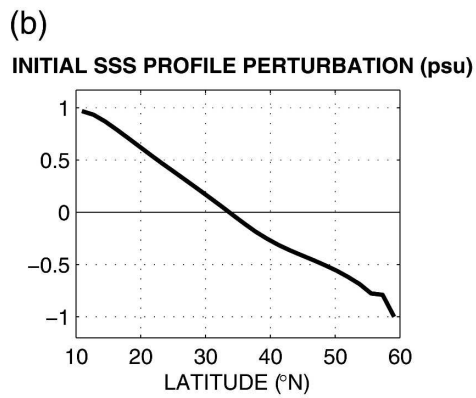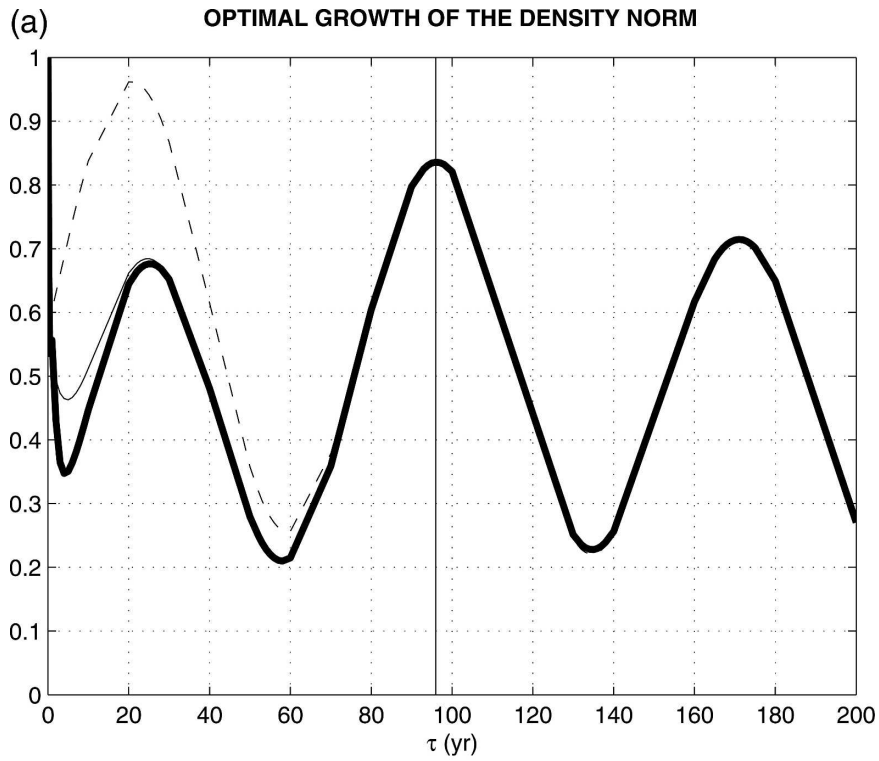
whose solution can be explicitly written as

$$|\mathbf{u}_0'\rangle = (2\gamma \mathbf{N})^{-1}\mathbf{H}_{ini}^C(\tau)|F\rangle, \quad (18)$$

where $\quad \mathbf{N} = \mathbf{P}^\dagger \mathbf{S}\mathbf{P}, \quad \mathbf{H}_{ini}^C(\tau) = \mathbf{P}^\dagger \mathbf{M}^\dagger(\tau), \quad$ and

$$\gamma = \pm\frac{1}{2}\sqrt{\langle F|\mathbf{H}_{ini}^{C\,\dagger}(\tau)\mathbf{N}^{-1}\mathbf{H}_{ini}^C(\tau)|F\rangle}. \quad (19)$$

This optimum is computed for different growth time τ. The largest values of the MOC intensity are obtained

(a)

OPTIMAL GROWTH OF THE DENSITY NORM

τ (yr)

(b)

INITIAL SSS PROFILE PERTURBATION (psu)

LATITUDE (°N)

(c)

DENSITY NORM GROWTH

TIME (yr)

(d)

$\alpha \times T'(96yr)$

DEPTH (m)

LATITUDE (°N)

(e)

$\beta \times S'(96yr)$

LATITUDE (°N)

(f)

$\Psi'(96yr)$ (Sv)

LATITUDE (°N)

for very small τ (Fig. 4), but these short time scales are not relevant in our 2D model and were ignored. Another maximum appears for $\tau = 67$ yr, which is in the time scale range that our model resolves. The transient growth results from both the nonnormality of the ocean dynamics and the quantity to be maximized. Actually, there is a measure that is always decaying with time and can be defined through the eigenmodes of the adjoint model (see below for its explicit formulation).

The optimal initial salinity profile and the corresponding perturbation of temperature, salinity, and overturning circulation after 67 yr are similar to those from the thermohaline density norm (Fig. 4). A linear time integration with the dipolar SSS perturbation used for initial conditions permits us to describe and understand the mechanisms leading to this strong finite-time growth, that is, the increase of the overturning intensity by a factor of 56 after 67 yr. Its physical mechanism is analogous to the one described in Sévellec et al. (2006) and consists of two ingredients. First, any salinity perturbation will be enhanced at the surface by a positive feedback occurring between the salinity forcing and the intensity of the circulation. Second, the initial salinity profile induces a reduction of the density meridional gradient, which decreases the circulation (1a), and the increase of the circulation only appears when the perturbation gradient reverses after having been advected, that is, after a delay of 67 yr. The conjunction of these two mechanisms explains why this perturbation profile is the most effective to modify the overturning circula-

tion. Moreover, this study enables the determination of an upper bound of the impact of SSS perturbation on the overturning circulation: no other 1-psu perturbation could have an impact greater than 7.7 Sv in a linear approximation. Observed interannual SSS anomalies in the Atlantic reach 0.2–0.3 psu in zonal average (Levitus 1989), for instance, within great salinity anomalies (Belkin et al. 1998). Our linear model would predict associated changes on the order of 2 Sv in the maximum overturning.

To better understand the two last analyses we propose an examination of the form of the solution in terms of the eigenmodes of the linearized tangent model $|\mathbf{u}_i\rangle$ (with associated eigenvalues λ_i), and of its adjoint $|\mathbf{u}_i^\dagger\rangle$ (with associated eigenvalues $\lambda_i^\dagger$). Using the property $\lambda_i^\dagger = \lambda_i^*$ (the asterisk denotes the complex conjugate) and the normalization convention $\langle\mathbf{u}_i|\mathbf{u}_j^\dagger\rangle = \delta_{ij}$ (δ_{ij} is the Kronecker function), we can decompose the two operators $\mathbf{A}$ and $\mathbf{A}^\dagger$ as

$$\mathbf{A} = \sum_i |\mathbf{u}_i\rangle\lambda_i\langle\mathbf{u}_i^\dagger| \quad \text{and} \quad \mathbf{A}^\dagger = \sum_i |\mathbf{u}_i^\dagger\rangle\lambda_i^*\langle\mathbf{u}_i|. \quad (20)$$

This very practical notation highlights the importance of each eigenmode. Removing the projection constraint as a first application, a norm maximization yields an eigenvalue problem like (14), $\mathbf{S}^{-1}\mathbf{M}^\dagger(\tau)\mathbf{S}\mathbf{M}(\tau)|\mathbf{u}\rangle = \gamma|\mathbf{u}\rangle$. Now, let us use the always-decaying norm briefly introduced previously and its inverse, which can be written, respectively, $\Sigma_i|\mathbf{u}_i^\dagger\rangle\langle\mathbf{u}_i^\dagger|$ and $\Sigma_i|\mathbf{u}_i\rangle\langle\mathbf{u}_i|$. The eigenvalue problem is then

$$\sum_{ij} |\mathbf{u}_i\rangle\langle\mathbf{u}_i|\mathbf{M}^\dagger(\tau)|\mathbf{u}_j^\dagger\rangle\langle\mathbf{u}_j^\dagger|\mathbf{M}(\tau) = \sum_{ijkl} |\mathbf{u}_i\rangle\langle\mathbf{u}_i|u_j^\dagger\rangle e^{\lambda_j^*\tau}\langle\mathbf{u}_j|\mathbf{u}_k^\dagger\rangle\langle\mathbf{u}_k^\dagger|\mathbf{u}_l\rangle e^{\lambda_l\tau}\langle\mathbf{u}_l^\dagger|$$

$$= \sum_{ijkl} |\mathbf{u}_i\rangle\delta_{ij}e^{\lambda_j^*\tau}\delta_{jk}\delta_{kl}e^{\lambda_l\tau}\langle\mathbf{u}_l^\dagger|$$

$$= \sum_i |\mathbf{u}_i\rangle e^{2\Re(\lambda_i)\tau}\langle\mathbf{u}_i^\dagger|.$$

The choice of this norm leads to an operator with eigenmodes $|\mathbf{u}_i\rangle$ and respective eigenvalues $\exp[2\Re(\lambda)\tau]$. In this case the eigenvalues problem solution (14) exhibits

maximum growth at time $\tau = 0$ only, because the steady state is stable; hence, all λ_i have negative real parts. This computation leads to two results—first, the inter-

$\leftarrow$

FIG. 3. (a) Maximum growth of the thermohaline density norm $[\langle\mathbf{u}(\tau)|\mathbf{S}|\mathbf{u}(\tau)\rangle]/[\langle\mathbf{u}(\tau)|\mathbf{S}|\mathbf{u}(\tau)\rangle]$ for initial salinity perturbations as a function of growth time τ. The thick, solid, and dashed lines correspond, respectively, to the tangent linear operator, and its truncation to 50 and 2 eigenvectors. The vertical solid line corresponds to the maximal growth at $\tau = 96$ yr, detailed in (b)–(f). (b) The optimal initial sea surface salinity profile, rescaled so that its absolute maximum equals 1 psu; and (c) time evolution of the density norm amplification $[\langle\mathbf{u}(t)|\mathbf{S}|\mathbf{u}(t)\rangle]/[\langle\mathbf{u}(0)|\mathbf{S}|\mathbf{u}(0)\rangle]$ in the linear model integration initialized with the optimal SSS perturbation; and (d) the temperature, (e) salinity (both scaled in terms of density), and (f) overturning (Sv) perturbation after 96 yr. The solid, dashed, and dotted lines, respectively, correspond to positive, negative, and zero anomalies; contour intervals are 2×10^{-5} in (d) and (e) and 1 Sv in (f).

(a)

OPTIMAL GROWTH OF THE MOC INTENSITY (Sv)

(b)

INITIAL SSS PROFILE PERTURBATION (psu)

(c)

MOC INTENSITY GROWTH

(d)

$\alpha \times T'(67\text{yr})$

(e)

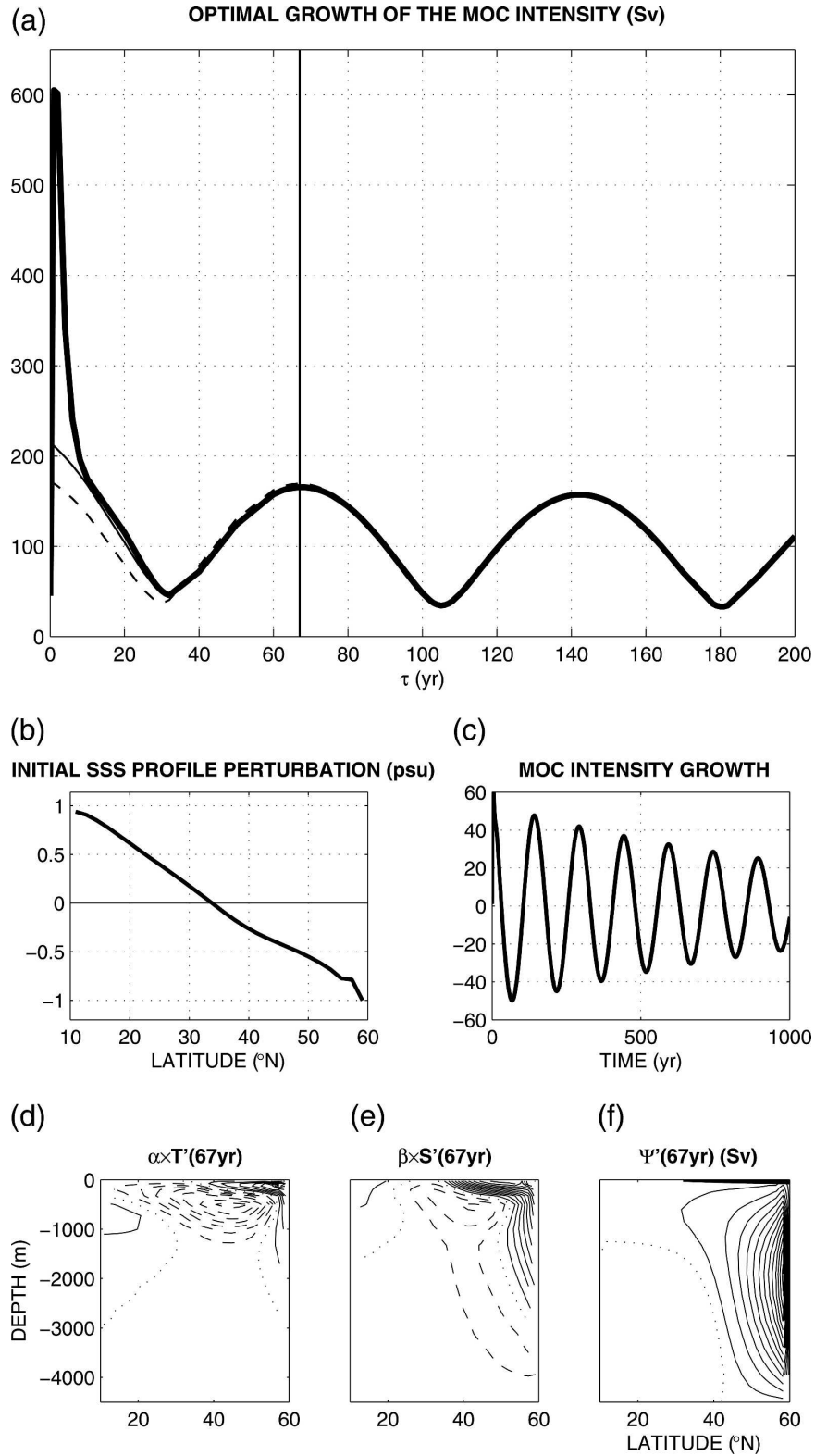$\beta \times S'(67\text{yr})$

(f)

$\Psi'(67\text{yr})$ (Sv)

FIG. 4. As in Fig. 3, but for the maximization of the overturning circulation intensity. (a) Optimal MOC intensity $\langle F|\mathbf{u}(\tau)\rangle$ for normalized initial SSS perturbation $\langle \mathbf{u}(0)|\mathbf{S}|\mathbf{u}(0)\rangle = 1$; the maximum growth appears at $\tau = 67$ yr, detailed in (b). (c) Time evolution of the MOC intensity amplification $[\langle F|\mathbf{u}(t)\rangle]/[\langle F|\mathbf{u}(0)\rangle]$ in the linear model integration is initialized with the optimal SSS perturbation. Contour intervals are 10^{-5} in (d) and (e) and 2 Sv in (f).
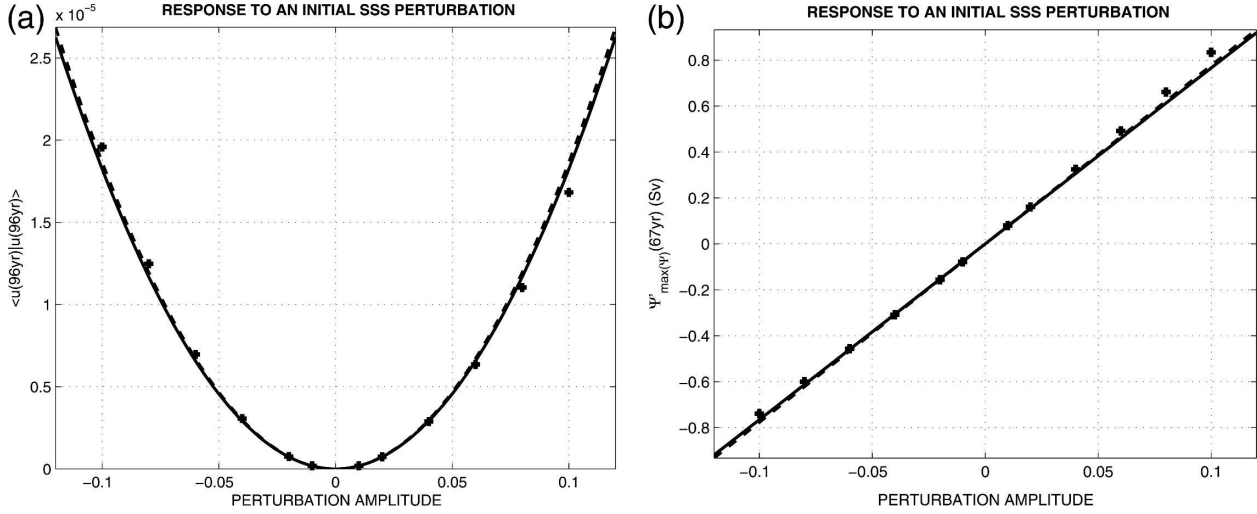
FIG. 5. Optimal growth of (a) the thermohaline density norm and (b) the overturning circulation intensity, as a function of the initial optimal perturbation amplitude, according to the theoretical computation (solid line), the linear (dashed line), and the nonlinear (crosses) time integrations.

est of such a decomposition notation in understanding the maximization problem, and second, the existence of a (although physically irrelevant) norm that is always decaying. This last result demonstrates that generalized stability analyses are measure dependent, and that the possible transient growth is only due to the choice of the measure. In the same way, we can rewrite the operators $\mathbf{H}_{\text{ini}}^N(\tau)$ and $\mathbf{H}_{\text{ini}}^C(\tau)$ as

$$\mathbf{H}_{\text{ini}}^N(\tau) = \mathbf{P}^\dagger \sum_{ij} e^{(\lambda_i^* + \lambda_j)\tau} |\mathbf{u}_i^\dagger\rangle\langle\mathbf{u}_i|\mathbf{S}|\mathbf{u}_j\rangle\langle\mathbf{u}_j^\dagger|\mathbf{P} \quad \text{and} \quad (21a)$$

$$\mathbf{H}_{\text{ini}}^C(\tau) = \mathbf{P}^\dagger \sum_i |\mathbf{u}_i^\dagger\rangle e^{\lambda_i^*\tau}\langle\mathbf{u}_i|. \quad (21b)$$

The last two sums reveal that the weight of each eigenmode is controlled by the product $\exp(\lambda_r\tau)$. Because our focus is on long time scales, we can truncate the sum, keeping only the leading eigenvalues to represent the linear tangent operator and its transpose. The complete sum corresponds to $N = 840$ (discretization of the salinity and temperature fields yields $N = 2n_yn_z$). We now provide the results from truncations to $N = 50$ and $N = 2$; both truncations correctly reproduce the long-time-scale results (Figs. 3a and 4a). At the time scales of the maximum growth (96 and 67 yr), the relative error does not exceed 5% for both truncations. In conclusion, only a couple of eigenmodes and their biorthogonals determine the effect of initial perturbations on long time scales. Consequently, the finite growth for both the thermohaline density norm and the MOC intensity is determined by the 150-yr oscillatory mode (Fig. 2). The finite-time growth is due to the projection of the least-damped oscillatory eigenmode of $\mathbf{A}^\dagger$ on the least-

damped oscillatory eigenmode of $\mathbf{A}$. We verified that the optimal perturbation corresponds to the surface salinity signature of a phase of the biorthogonal of the 150-yr oscillatory mode. Maximum growth appears every 75 yr, which corresponds to the half-period delay between most efficient phases of the perturbation (opposite perturbations yield identical growth).

To confirm these results, we integrate in time the linearized model initialized by the optimal perturbation with varying amplitudes. Moreover, to validate a posteriori the linear approach, we also conduct a time integration of the nonlinear model initialized by the same optimal perturbations (for both the thermohaline density norm and for the MOC intensity analysis). The optimal growth for the theoretical computation is very close to both the linear and nonlinear time integration for SSS perturbations up to 0.1 psu (Fig. 5). This last result somehow confirms the validity of our approximations for time scales of the order of a few centuries, and shows the legitimacy range of the linear study. However, we only validate the growth of our optimal initial SSS here; we do not check whether this optimal initial SSS is the optimal perturbation in the nonlinear model (Mu and Zhang 2006).

6. Optimal constant surface salinity flux

On our way to investigate the response of a stable steady state to a perturbation, we now study a constant surface salinity flux (SSF) perturbation. Thus, we address the second question: what is the optimal constant perturbation of the surface salinity flux that induces the

largest variation of the thermohaline circulation? Again we will consider both the thermohaline norm and the meridional overturning intensity. The time evolution of the perturbation now reads

$$d_t|\mathbf{u}\rangle = \mathbf{A}|\mathbf{u}\rangle + |\mathbf{f}\rangle, \tag{22}$$

where $|\mathbf{f}\rangle$ is the permanent forcing perturbation. After integration, this equation leads to

$$|\mathbf{u}(\tau)\rangle = \mathbf{M}(\tau)|\mathbf{u}(0)\rangle + \int_0^\tau ds\, \mathbf{M}(\tau - s)|\mathbf{f}\rangle = \int_0^\tau ds\, \mathbf{M}(\tau - s)|\mathbf{f}\rangle, \tag{23}$$

where we assume, without loss of generality, that the initial perturbation verifies $|\mathbf{u}(0)\rangle = 0$ (the optimal initial perturbation is computed in the previous section). The Lagrangian function can then be written

$$\mathcal{L}_{\mathrm{cst}}^N = \langle \mathbf{u}(\tau)|\mathbf{S}|\mathbf{u}(\tau)\rangle - \gamma(\langle \mathbf{f}|\mathbf{S}|\mathbf{f}\rangle - 1). \tag{24}$$

Because we are interested in permanent modifications, the algebra is conducted in the limit $\tau \to \infty$. Using the following notations with $|\mathbf{f}\rangle = \mathbf{P}|\mathbf{f}'\rangle$:

$$\mathbf{H}_{\mathrm{cst}}^N(\infty) = \lim_{\tau \to \infty} \int_0^\tau ds \int_0^\tau ds'\, \mathbf{P}^\dagger \mathbf{M}^\dagger(\tau - s')\mathbf{S}\mathbf{M}(\tau - s)\mathbf{P} \tag{25}$$

and

$$\mathbf{N} = \mathbf{P}^\dagger \mathbf{S}\mathbf{P}, \tag{26}$$

the maximization problem leads to the eigenvalue problem,

$$\mathbf{N}^{-1}\mathbf{H}_{\mathrm{cst}}^N(\infty)|\mathbf{f}'\rangle = \gamma|\mathbf{f}'\rangle. \tag{27}$$

The eigenmode with the largest real part corresponds to the optimal SSF profile (Fig. 6). The linear temperature, salinity, and overturning circulation perturbations in the permanent regime are computed from a linear time integration forced by this profile over 10 000 yr, at which time all of the transient growth is damped (Fig. 6).

We now seek the optimal permanent surface salinity flux leading to the largest change of the overturning circulation intensity. The Lagrangian reads

$$\mathcal{L}_{\mathrm{cst}}^C = \langle \mathbf{F}|\mathbf{u}(\tau)\rangle - \gamma(\langle \mathbf{f}|\mathbf{S}|\mathbf{f}\rangle - 1). \tag{28}$$

Using the notation

$$\mathbf{H}_{\mathrm{cst}}^C(\infty) = \lim_{\tau \to \infty} \int_0^\tau ds\, \mathbf{P}^\dagger \mathbf{M}^\dagger(\tau - s), \tag{29}$$

we find

$$\gamma = \pm \frac{1}{2}\sqrt{\mathbf{H}_{\mathrm{cst}}^{C\,\dagger}(\infty)\mathbf{N}^{-1}\mathbf{H}_{\mathrm{cst}}^C(\infty)}, \tag{30}$$

where $\mathbf{N} = \mathbf{P}^\dagger \mathbf{S}\mathbf{P}$. The explicit solution reads $|\mathbf{f}'\rangle = (2\gamma \mathbf{N})^{-1}\mathbf{H}_{\mathrm{cst}}^C(\infty)|\mathbf{F}\rangle$. The optimal SSF profile, as well as the linear temperature, salinity, and overturning circulation perturbations in the permanent regime strongly differ from the previous norm (Fig. 6). This linear analysis provides an upper bound of the SSF impact on the overturning intensity: a modification of 1 psu yr^{-1}, equivalent to a freshwater flux perturbation of 1.43 m yr^{-1}, leads to a response of 6.5 Sv, impeding the existence of any greater modification. For instance, global warming is expected to increase the hydrological cycle on the order of 4% within the next century (Held and Soden 2006); such changes would result in a 3 cm yr^{-1} freshwater flux change in our model, and hence an impact on the order of 0.14 Sv in the overturning within our linear framework. We understand this perturbation mechanism as follows: the constant SSF counterbalances the salinity forcing of the steady state and so indirectly increases the effect of temperature gradient on the circulation, which is accordingly intensified. As seen in Fig. 6a, the strong local gradient in the north, just at the top of the overturning streamfunction maximum of the steady state, is a very effective way for a perturbation to modify the circulation intensity.

As done before we rewrite the tangent linear operator and its adjoint in terms of their eigenmodes,

$$\mathbf{H}_{\mathrm{cst}}^N(\infty)\mathbf{P}^\dagger \sum_{ij} \frac{1}{\lambda_i^* \lambda_j}|\mathbf{u}_i^\dagger\rangle\langle \mathbf{u}_i|\mathbf{S}|\mathbf{u}_j\rangle\langle \mathbf{u}_j^\dagger|\mathbf{P} \tag{31a}$$

for the thermohaline density norm and

$$\mathbf{H}_{\mathrm{cst}}^C(\infty) = -\mathbf{P}^\dagger \sum_i \frac{|\mathbf{u}_i^\dagger\rangle\langle \mathbf{u}_i|}{\lambda_i^*} \tag{31b}$$

for the maximum overturning circulation function. Note that every eigenmode is weighted by the inverse of its eigenvalue $(1/\lambda)$, which is less discriminating than the factor $\exp(\lambda \tau)$ derived for the optimal initial perturbation. As one can thus expect, the truncation is a very bad approximation in this context; actually, all of the eigenmodes have an impact on the solution of the optimal forcing perturbation.

We also compare the theoretical result with the outcome of both linear and nonlinear 10 000-yr-long time integrations for varying amplitude perturbations (Fig. 7). The three results are in good agreement for the thermohaline density norm. A difference appears in the MOC intensity, however, the relative error remains lower than 12%. This discrepancy may come from the relatively crude approximation that we use to estimate the MOC intensity averaged over several grid points.
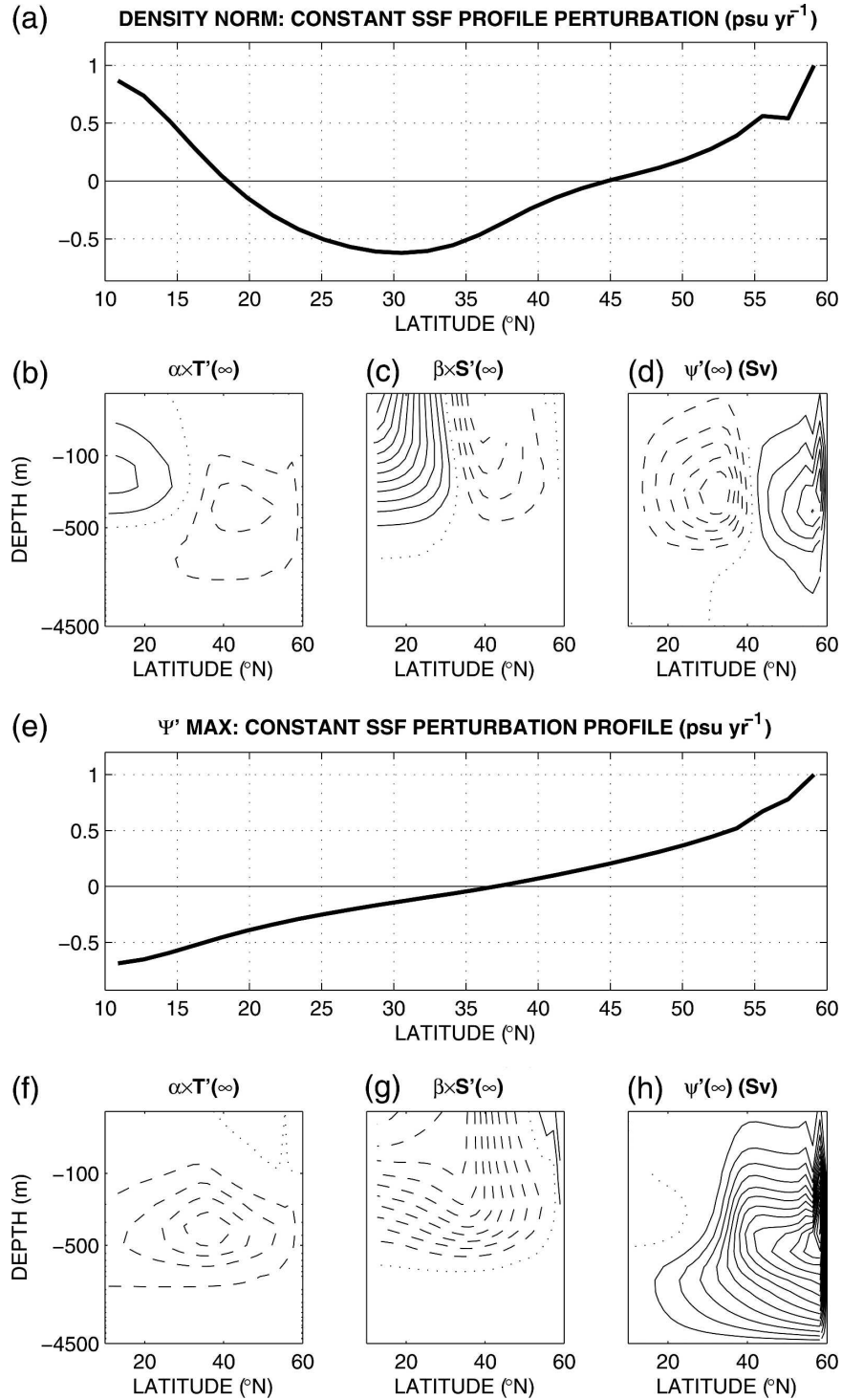
(a)
DENSITY NORM: CONSTANT SSF PROFILE PERTURBATION (psu yr^{-1})

(b) $\alpha \times$**T'**(∞) (c) $\beta \times$**S'**(∞) (d) $\psi'(\infty)$ **(Sv)**

(e)
Ψ' MAX: CONSTANT SSF PERTURBATION PROFILE (psu yr^{-1})

(f) $\alpha \times$**T'**(∞) (g) $\beta \times$**S'**(∞) (h) $\psi'(\infty)$ **(Sv)**

FIG. 6. (a), (e) Optimal constant surface salinity flux perturbation inducing the largest modification of the (a)–(d) thermohaline density norm and (e)–(h) overturning circulation intensity in a stationary regime ($\tau \rightarrow \infty$). Perturbations have been scaled for a maximum absolute value of 1 psu. (b), (f) Temperature, (c), (g) salinity (both scaled in terms of density), and (d), (h) overturning (Sv) perturbations after 10 000 yr (stationary regime). The solid, dashed, and dotted lines, respectively, correspond to positive, negative, and zero anomalies; contour intervals are 1.5×10^{-4} in (b), (c), (f), and (g) and 0.5 Sv in (d) and (h). A logarithmic scale is used on the vertical.
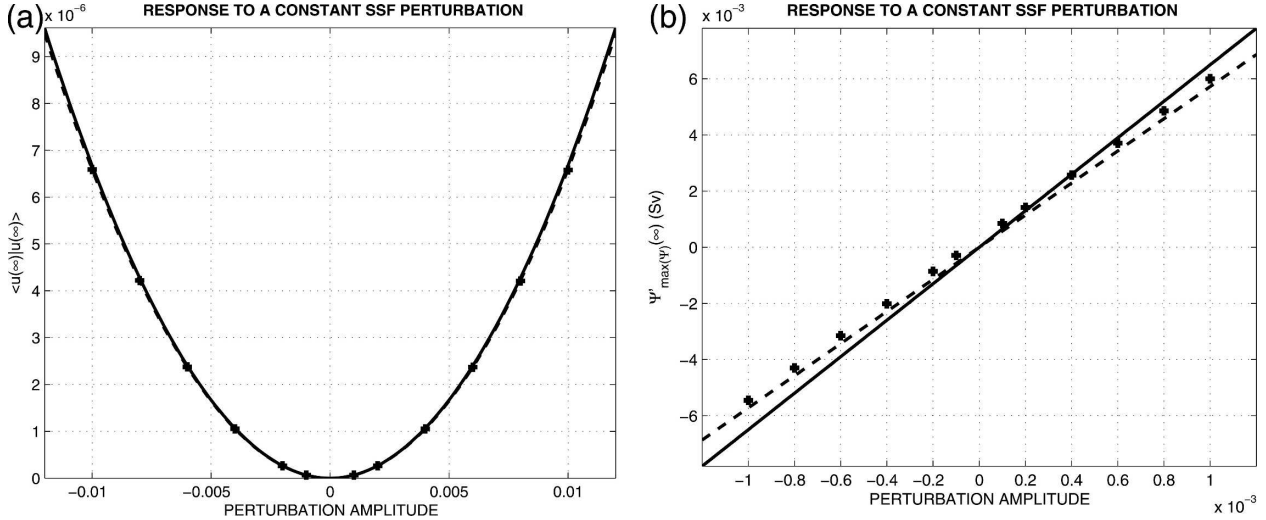
FIG. 7. As in Fig. 5, but for the constant surface salinity flux perturbation of (a) the thermohaline density norm and (b) the thermohaline circulation intensity. The relative error between the different computations remains lower than 12%.

7. Optimal stochastic surface salinity flux

In the last step of this study, we investigate the influence of stochastic time-dependent perturbations inducing variability around the stable steady state (Farrell and Ioannou 1993). We thus address the last question: what is the optimal spatial structure of the stochastic surface salinity flux, which induces the largest response of the thermohaline circulation in terms of variance? The time evolution of the perturbations now reads

$$d_t|\mathbf{u}(t)\rangle = \mathbf{A}|\mathbf{u}(t)\rangle + |\mathbf{f}(t)\rangle, \tag{32}$$

where $|\mathbf{f}(t)\rangle$ is the stochastic time-dependent forcing. The time integration leads to

$$|\mathbf{u}(\tau)\rangle = \mathbf{M}(\tau)|\mathbf{u}(0)\rangle + \int_0^\tau ds\, \mathbf{M}(\tau - s)|\mathbf{f}(s)\rangle. \tag{33}$$

Without loss of generality, we can assume $|\mathbf{u}(0)\rangle = 0$. It is convenient to assume a separable form for the forcing, $|\mathbf{f}(t)\rangle = a(t)|\mathbf{g}\rangle$, where $a(t)$ is the stochastic part of our perturbation and $|\mathbf{g}\rangle$ is the time-independent me-

ridional profile. Because the thermohaline circulation time scales are much longer than the atmospheric ones, the forcing variations can reasonably be approximated by white noise. The autocorrelation function of the stochastic forcing intensity is thus the classical delta function $E[a(t)a(t')] = \delta(t - t')$, where E denotes the expected value. We can then rewrite the time perturbation dependence as

$$|\mathbf{u}(\tau)\rangle = \int_0^\tau ds\, a(s)\mathbf{M}(\tau - s)|\mathbf{g}\rangle. \tag{34}$$

We seek the two spatial profiles of the optimal stochastic forcing perturbation that maximize the variance of the state vector and the variance of the MOC intensity. For the first case, the Lagrangian is

$$\mathcal{L}_{\text{sto}}^N = \text{var}[|\mathbf{u}(\tau)\rangle] - \gamma(\langle\mathbf{g}|\mathbf{S}|\mathbf{g}\rangle - 1). \tag{35}$$

With the variance of the state vector being norm dependent, as before we use the thermohaline norm in terms of density,

$$
\begin{aligned}
\text{var}[|\mathbf{u}(\tau)\rangle] &= E[\langle\mathbf{u}(\tau)|\mathbf{S}|\mathbf{u}(\tau)\rangle] - \langle E[\mathbf{u}(\tau)]|\mathbf{S}|E[\mathbf{u}(\tau)]\rangle \\
&= E[\langle\mathbf{u}(\tau)|\mathbf{S}|\mathbf{u}(\tau)\rangle] \\
&= \left\langle \mathbf{g}\left| \int_0^x ds \int_0^x ds'\, E[a(s)a(s')]\mathbf{M}^\dagger(\tau - s)\mathbf{S}\mathbf{M}(\tau - s')\right|\mathbf{g} \right\rangle \\
&= \left\langle \mathbf{g}\left| \int_0^x ds\, \mathbf{M}^\dagger(\tau - s)\mathbf{S}\mathbf{M}(\tau - s')\right|\mathbf{g} \right\rangle. \tag{36}
\end{aligned}
$$

Using the following notations and $|g\rangle = P|g'\rangle$:

$$H_{sto}^N(\infty) = \lim_{\tau \to \infty} \int_0^\tau ds\, P^\dagger M^\dagger(\tau - s)SM(\tau - s)P \quad \text{and} \tag{37}$$

$$N = P^\dagger SP, \tag{38}$$

the maximization problem results in the eigenvalue problem,

$$N^{-1}H_{sto}^N(\infty)|g'\rangle = \gamma|g'\rangle. \tag{39}$$

The eigenmode with the largest real part corresponds to the optimal stochastic profile (Fig. 8a); it varies linearly with latitude and conserves the total salt, with the same shape as the ones found for the optimal initial salinity perturbations (section 5). A linear time integration forced by this profile with a white-noise amplitude reveals the variability of the state vector norm as represented in Fig. 8b. The power spectral density of this variability (Fig. 9a), which is norm dependent, reveals a red noise with a peak of around 150 yr; as expected, this spectral peak coincides exactly with the period of the least-damped internal mode. To better understand this

power spectral density we compute it analytically (Ioannou 1995), defining $|\hat{u}(\omega)\rangle$ as the Fourier transform of $|u(t)\rangle$ and $\langle\hat{u}(\omega)|$ as its complex conjugate transpose (which is different from the Fourier transform of $\langle u(t)|$), and we obtain [using (32)] the following relation:

$$i\omega|\hat{u}(\omega)\rangle = A|\hat{u}(\omega)\rangle + |g\rangle. \quad \text{That is,}$$

$$|\hat{u}(\omega)\rangle = (i\omega I - A)^{-1}|g\rangle. \tag{40}$$

We are now able to derive the analytical expression of the power spectral density,

$$\begin{aligned} \text{psd}^N(\omega) &= \langle\hat{u}(\omega)|S|\hat{u}(\omega)\rangle \\ &= \langle g|(-i\omega I - A^\dagger)^{-1}S(i\omega I - A)^{-1}|g\rangle. \end{aligned} \tag{41}$$

This theoretical result corresponds exactly to the power spectrum numerically computed from the direct time integration (Fig. 9a).

Proceeding to the variance of the overturning circulation intensity, the function to maximize becomes

$$\mathcal{L}_{sto}^C = \text{var}[\langle F|u(\tau)\rangle] - \gamma(\langle g|S|g\rangle - 1). \tag{42}$$

This variance can be rewritten as

$$\begin{aligned} \text{var}[\langle F|u(\tau)\rangle] &= E[\langle F|u(\tau)\rangle^2] - \langle F|[u(\tau)]\rangle^2 = E[\langle F|u(\tau)\rangle^2] \\ &= \langle g|\int_0^\tau ds \int_0^\tau ds'\, E[a(s)a(s')]M^\dagger(\tau - s)|F\rangle\langle F|M(\tau - s')|g\rangle \\ &= \langle g|\int_0^\tau M^\dagger(\tau - s)|F\rangle\langle F|M(\tau - s)\, ds\, |g\rangle. \end{aligned} \tag{43}$$

Using the following notations:

$$H_{sto}^C(\infty) = \lim_{\tau \to \infty} \int_0^\tau ds\, P^\dagger M^\dagger(\tau - s)|F\rangle\langle F|M(\tau - s)P, \quad \text{and}$$

$$N = P^\dagger SP, \tag{44}$$

the maximization problem reduces to the eigenvalue problem:

$$N^{-1}H_{sto}^C(\infty)|g'\rangle = \gamma|g'\rangle. \tag{45}$$

The optimal stochastic profile is the eigenmode with the largest real part (Fig. 8c) and is identical to the one with the previous norm. This profile is the same as the one for the optimal initial SSS perturbations. It is the most efficient initial structure to provide the largest circulation intensity change; then, when stochastically forced, one can expect that it remains the most efficient structure to continuously sustain the largest circulation

intensity variability. As verified in a linear time integration (Fig. 8d), the optimal stochastic surface salinity (freshwater) flux profile for a 1 psu yr^{-1} (1.43 m yr^{-1}) standard deviation induces a standard deviation of 133 Sv; this is the upper bound of the circulation intensity response to stochastic salinity forcing in the linear approximation. Subannual variability of the freshwater flux zonally averaged over the Atlantic Ocean may be roughly estimated from atmospheric reanalysis such as either the National Centers for Environmental Prediction–National Center for Atmospheric Research (NCEP–NCAR) reanalysis or the 40-yr European Centre for Medium-Range Weather Forecasts (ECMWF) reanalysis (ERA-40); it is of the order of 5 cm yr^{-1} in midlatitudes. In our model this would lead to a standard deviation of the overturning intensity of 4.6 Sv.

The power spectral density of this variability (Fig. 9b) reveals a red noise and a peak around 150 yr, coinciding exactly with the period of the least-damped internal mode. As done above, we derive an analytical expression for the power spectral density,

(a)   **DENSITY NORM: STOCHASTIC SSF PERTURBATION PROFILE (psu $\bar{y}r^{-1}$)**

(b)   **$\langle u(t)|u(t)\rangle \Rightarrow Var(|u(t)\rangle)=0.739$**

(c)   **Ψ' MAX: STOCHASTIC SSF PERTURBATION PROFILE (psu $\bar{y}r^{-1}$)**

(d)   **$\Psi'_{max(\Psi)}(t)$ (Sv) $\Rightarrow Var(\Psi'_{max(\Psi)}(t))=17831$ Sv^2**
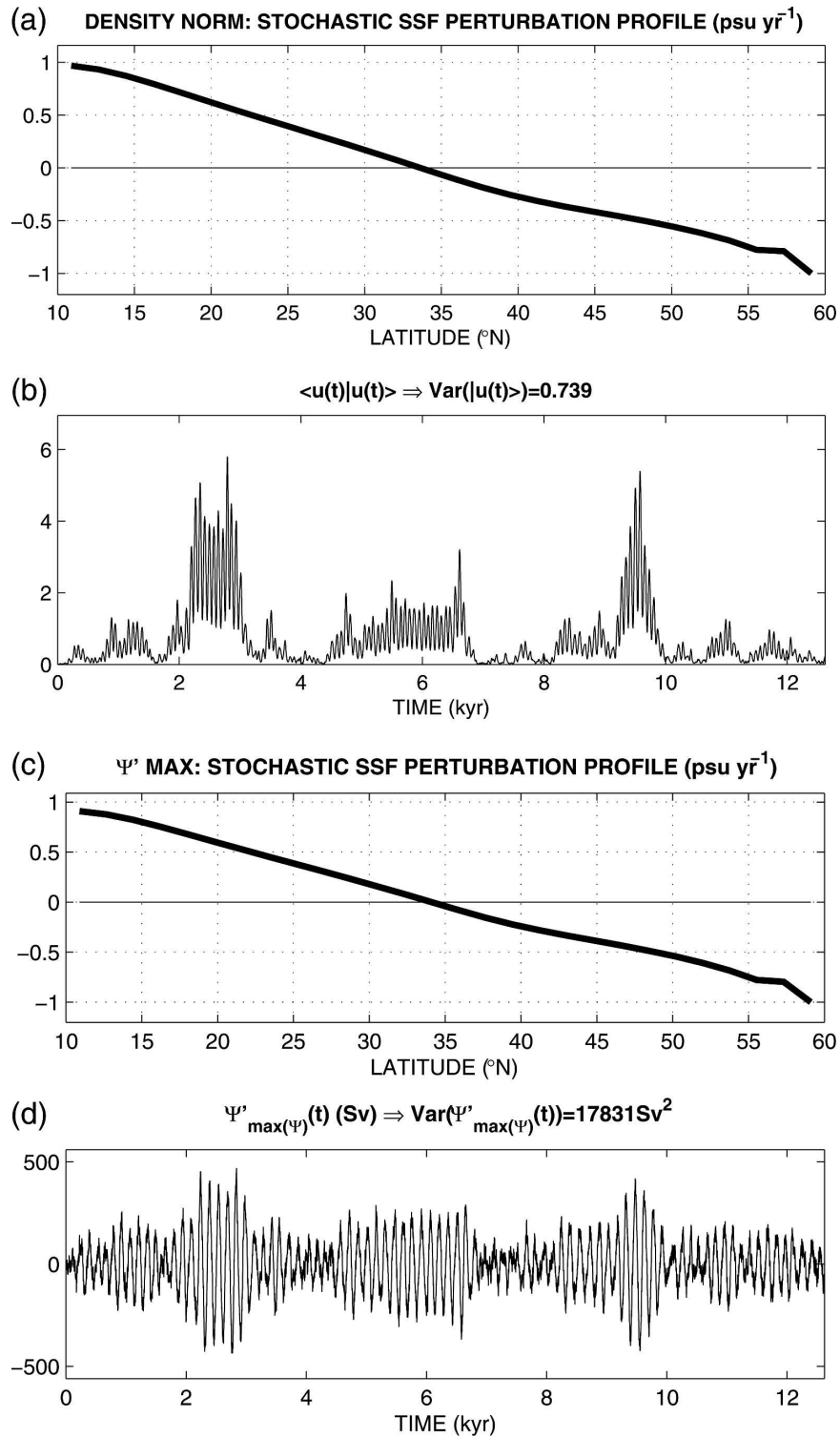
FIG. 8. Optimal stochastic surface salinity flux perturbation inducing the largest variance (a) defined by the thermohaline density norm, and (c) of the overturning circulation intensity, in a permanent regime ($\tau \rightarrow \infty$). Stochastic perturbations have been scaled such that the standard deviation is 1 psu yr^{-1}. (b), (d) Thermohaline density norm and overturning circulation intensity during a linear time integration forced by their respective stochastic optimals.
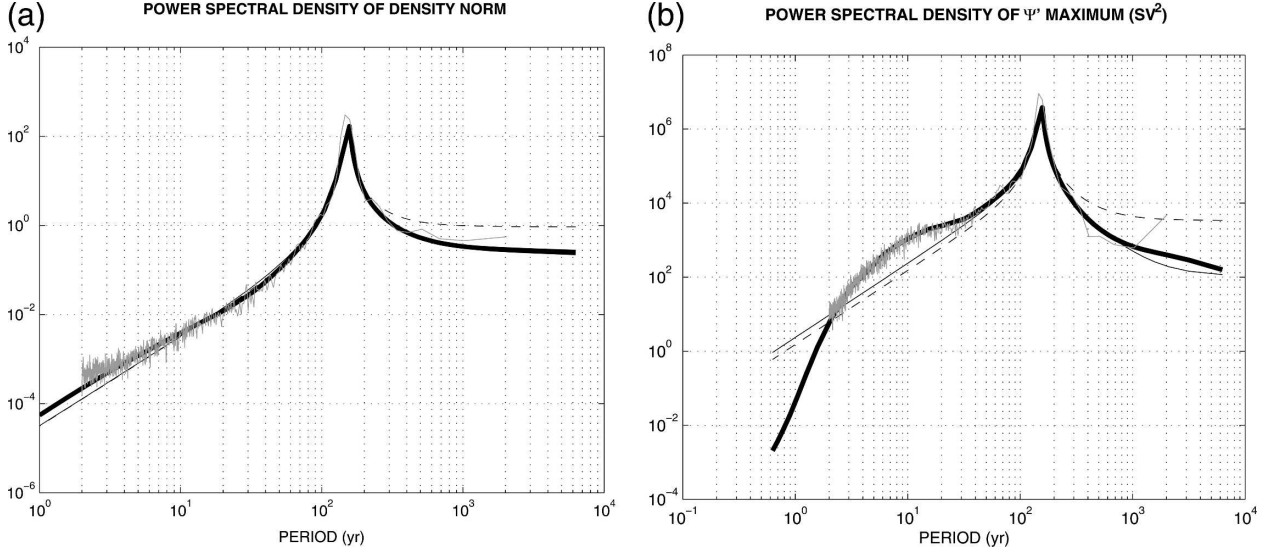
FIG. 9. Power spectral density (a) defined by the density norm and (b) of the overturning circulation intensity. The theoretical spectrum (thick line) is compared with the truncation at 50 (solid line) and 2 (dashed line) eigenmodes and to the perturbed linear time integration spectrum (gray line). In both cases the weakly damped 150-yr oscillation eigenmode controls the intensity of the spectrum.

$$\mathrm{psd}^C(\omega) = \langle \hat{\mathbf{u}}(\omega)| \rangle \langle F | \hat{u}(\omega) \rangle$$

$$= \langle \mathbf{g} | (-i\omega \mathbf{I} - \mathbf{A}^\dagger)^{-1} | F \rangle \langle F | (-i\omega \mathbf{I} - \mathbf{A}^\dagger)^{-1} | \mathbf{g} \rangle. \tag{46}$$

This theoretical result confirms a peak corresponding to the least-damped mode (Fig. 8a,b).

Again, it is convenient to rewrite the tangent linear operator and its adjoint in terms of their eigenmodes, leading to the following expressions:

$$\mathbf{H}_{\mathrm{sto}}^N(\infty) = \mathbf{P}^\dagger \sum_{ij} \frac{-1}{\lambda_i^* + \lambda_j} |\mathbf{u}_i^\dagger\rangle \langle \mathbf{u}_i | \mathbf{S} | u_j \rangle \langle u_j^\dagger | \mathbf{P} \tag{47a}$$

for the thermohaline density norm and

$$\mathbf{H}_{\mathrm{sto}}^C(\infty) = \mathbf{P}^\dagger \sum_{ij} \frac{-1}{\lambda_i^* + \lambda_j} |\mathbf{u}_i^\dagger\rangle \langle \mathbf{u}_i | F \rangle \langle F | \mathbf{u}_j \rangle \langle \mathbf{u}_j^\dagger | \mathbf{P} \tag{47b}$$

for the overturning circulation intensity. Every couple of eigenmodes is associated with the inverse of its respective eigenvalue sum. When a truncation of the sum to the leading two eigenmodes is performed, the error of the expected variance is only about 5.5% for both the density norm and maximum overturning circulation function. Using the same decomposition, the power spectral densities (41) and (46) can be rewritten as

$$\mathrm{psd}^N(\omega) = \sum_{ij} \langle \mathbf{g} | \mathbf{u}_j^\dagger \rangle \frac{1}{-i\omega - \lambda_i^*} \langle \mathbf{u}_i | \mathbf{S} | \mathbf{u}_j \rangle \langle \mathbf{u}_j^\dagger | \mathbf{g} \rangle, \tag{48a}$$

$$\mathrm{psd}^C(\omega) = \sum_{ij} \langle \mathbf{g} | \mathbf{u}_j^\dagger \rangle \frac{1}{-i\omega - \lambda_i^*} \langle \mathbf{u}_i |$$

$$\times \langle F | \mathbf{u}_j \rangle \frac{1}{i\omega - \lambda_j} \langle \mathbf{u}_j^\dagger | \mathbf{g} \rangle, \quad \text{and} \tag{48b}$$

$$|\hat{\mathbf{u}}(\omega)\rangle = \sum_i |\mathbf{u}_i\rangle \frac{1}{i\omega - \lambda_i} \langle \mathbf{u}_i^\dagger | \mathbf{g} \rangle. \tag{49}$$

These power spectral densities are represented in Fig. 9 for a truncation to 50 and 2 eigenmodes. It appears that the dynamics of the variance are mainly controlled by a few eigenmodes, moreover the peak is explained by only two eigenmodes corresponding to the weakly damped 150-yr oscillation.

We finally repeat the comparison of the theoretical solution with linear and nonlinear direct time integrations forced by stochastic perturbations of varying amplitudes for 12 000 yr (Fig. 10). The three results are in good agreement for the thermohaline density norm. However, while some differences appear in the overturning circulation intensity, the relative error in standard deviation remains lower than 20%.

8. Conclusions

In the context of the ocean response to climate warming, we investigated the influence of perturbations
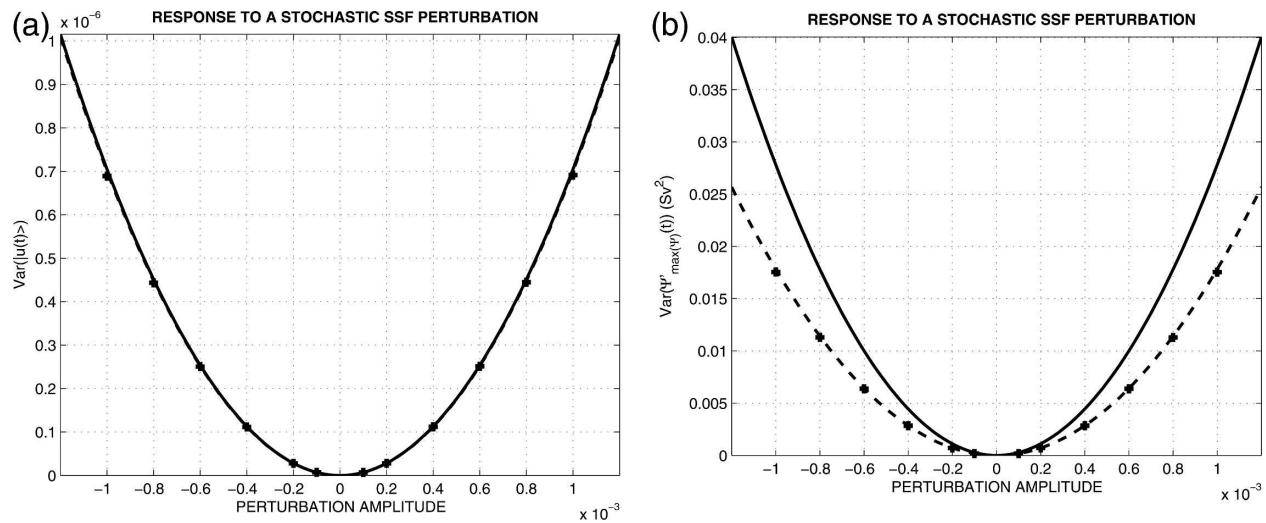
FIG. 10. As in Fig. 5, but for the optimal stochastic surface salinity flux of (a) the thermohaline density norm and (b) the thermohaline circulation intensity. The relative error in standard deviation between the different computations remains lower than 20%.

of sea surface salinity and freshwater flux on the thermohaline circulation, the slow component of the climate system transporting heat poleward. Three types of optimal perturbations are addressed: initial sea surface salinity perturbation, and constant and stochastic salinity forcing perturbations. Numerical solutions are found using a 2D latitude–depth model. The solutions provide upper bounds for the amplitude of the thermohaline circulation response.

To evaluate the change of the thermohaline circulation we have compared two measures—a thermohaline density norm and the intensity of the thermohaline circulation. Analytical solutions for the optimal profiles read as an eigenvalue problem in the former case, but an explicit solution for the latter. Although the second measure is not accurately defined, it induces more interesting results because it has more physical meaning for the ocean role in climate than the thermohaline density norm. The optimal response is intrinsically related to the quantity we maximize. Actually, the norm based on the eigenvalues of the adjoint model cannot exhibit finite-time growth. We stress here that such studies are strongly dependent on the choice of the measure.

The initial sea surface salinity perturbation maximizing the thermohaline circulation intensity is simply a linear profile with latitude. We found a maximum transient growth after 67 yr due to a positive feedback between surface salinity forcing and advection inducing a reinforcement of salinity perturbation at the surface (Marotzke 1996). For the salinity forcing perturbation maximizing the same measure, the classical way to modify the circulation is confirmed, that is, a decrease

in the amplitude of the freshwater flux enhances the temperature-dominated density gradient and thus increases the circulation intensity. The optimal stochastic salinity forcing perturbation shows the same large-scale structure as that of the optimal initial SSS perturbation; this result is not inconsistent because this profile, stochastically forced, continuously provides the largest variability of the circulation intensity. This analysis highlights the preponderance of the most weakly damped 150-yr-period linear mode to explain the major part of the variability spectrum of the circulation intensity response, and more particularly the apparition of a 150-yr frequency peak. Each of these three analyses of optimal salinity perturbations provides upper bounds for the oceanic response in a linear approximation: a 0.2-psu maximum initial surface salinity perturbation cannot modify the overturning intensity by more than 2 Sv; a 3 cm yr^{-1} maximum freshwater flux cannot change the overturning by more than 0.14 Sv; and a stochastic freshwater flux with a 5 cm yr^{-1} maximum standard deviation induces an overturning intensity standard deviation of 4.6 Sv. Given such observed or expected perturbations of surface salinity and freshwater flux, the variability of the thermohaline circulation in this 2D model appears plausible for upper bounds.

Moreover, the first and the third analysis can be largely explained by a few damped eigenmodes provided by the linear and adjoint stability analysis of our reference stable steady state. This approximation has been theoretically computed and numerically confirmed. This last result means that only a finite number of the least-damped eigenmodes and their biorthogonals contributes effectively to the low-frequency vari-

ability, which suggests the feasibility of further applications in more realistic models.

The application of the maximization method to this idealized 2D model is seen as a first methodological step that is now being extended to a 3D realistic global model to obtain optimal structures and associated upper bounds of the ocean circulation response. The explicit optimal solutions for the initial and constant forcing perturbations should be especially tractable in more complex models. Another possible extension is to address nonlinear behavior, because several recent papers (Mu et al. 2004; Sun et al. 2005; Mu and Zhang 2006) suggest that the linear approximation may be a strong limitation in a such study. Actually, even if the linear evolution of the optimal perturbation is close to its nonlinear evolution for weak perturbations, this does not mean that the optimal pattern found through the tangent linear model is close to the one found with the fully nonlinear model. Last, dealing with sea surface salinity perturbations may require a better representation of the water cycle through the coupling to atmosphere and ice models; such an implementation can be a very interesting continuation to this work.

REFERENCES

Belkin, I. S., S. Levitus, J. Antonov, and S.-A. Malmberg, 1998: Great Salinity Anomalies in the North Atlantic. *Prog. Oceanogr.,* **41,** 1–68.

Colin de Verdière, A., M. Ben Jelloul, and F. Sévellec, 2006: Bifurcation structure of thermohaline oscillation. *J. Climate,* **19,** 5777–5795.

Curry, R., and C. Mauritzen, 2005: Dilution of the northern North Atlantic Ocean in recent decades. *Science,* **308,** 1772–1774.

——, B. Dickson, and I. Yashayaev, 2003: A change in freshwater balance of the Atlantic Ocean over the past four decades. *Nature,* **426,** 826–829.

Farrell, B. F., and A. M. Moore, 1992: An adjoint method for obtaining the most rapidly growing perturbation to oceanic flows. *J. Phys. Oceanogr.,* **22,** 338–349.

——, and P. J. Ioannou, 1993: Stochastic forcing of perturbation variance in unbounded shear and deformation flows. *J. Atmos. Sci.,* **50,** 200–211.

——, and ——, 1996: Generalized stability theory. Part I: Autonomous operators. *J. Atmos. Sci.,* **53,** 2025–2040.

Griffies, S. M., and E. Tziperman, 1995: A linear thermohaline oscillator driven by stochastic atmospheric forcing. *J. Climate,* **8,** 2440–2453.

Held, I. M., and B. J. Soden, 2006: Robust responses of the hydrological cycle to global warming. *J. Climate,* **19,** 5686–5699.

Huck, T., and G. K. Vallis, 2001: Linear stability analysis of three-dimensional thermally-driven ocean circulation: Application to interdecadal oscillations. *Tellus,* **53A,** 526–545.

Ioannou, P. J., 1995: Nonnormality increases variance. *J. Atmos. Sci.,* **52,** 1155–1158.

Josey, S. A., and R. Marsh, 2005: Surface freshwater flux variability and recent freshening of the North Atlantic in the eastern subpolar gyre. *J. Geophys. Res.,* **110,** C05008, doi:10.1029/2004JC002521.

Levitus, S., 1989: Interpentadal variability of temperature and salinity at intermediate depths of the North Atlantic Ocean, 1970–1974 versus 1955–1959. *J. Geophys. Res.,* **94,** 6091–6131.

Lohmann, G., and J. Schneider, 1999: Dynamics and predictability of Stommel's box model. A phase-space perspective with implications for decadal climate variability. *Tellus,* **51A,** 326–336.

Marotzke, J., 1996: Analysis of thermohaline feedbacks. *Decadal Climate Variability: Dynamics and Predictability,* D. L. T. Anderson and J. Willebrand, Eds., NATO ASI Series I, Vol. 44, Springer, 333–378.

——, and J. R. Scott, 1999: Convective mixing and the thermohaline circulation. *J. Phys. Oceanogr.,* **29,** 2962–2970.

——, P. Welander, and J. Willebrand, 1988: Instability and multiple steady states in a meridional-plane model of the thermohaline circulation. *Tellus,* **40A,** 162–172.

Mikolajewicz, U., and E. Maier-Reimer, 1990: Internal secular variability in an ocean general circulation model. *Climate Dyn.,* **4,** 145–156.

Moore, A. M., and B. F. Farrell, 1993: Rapid perturbation growth on spatially and temporally varying oceanic flows determined using an adjoint method: Application to the Gulf Stream. *J. Phys. Oceanogr.,* **23,** 1682–1702.

——, C. L. Perez, and J. Zavala-Garay, 2002: A non-normal view of the wind-driven ocean circulation. *J. Phys. Oceanogr.,* **32,** 2681–2705.

——, J. Vilard, A. T. Weaver, D. L. T. Anderson, R. Kleeman, and J. R. Johnson, 2003: The role of air–sea interaction in controlling the optimal perturbations of low-frequency tropical coupled ocean–atmosphere modes. *J. Climate,* **16,** 951–968.

Mu, M., and Z. Zhang, 2006: Conditional nonlinear optimal perturbations of a two-dimensional quasigeostrophic model. *J. Atmos. Sci.,* **63,** 1587–1604.

——, L. Sun, and H. A. Dijkstra, 2004: The sensitivity and stability of the ocean's thermohaline circulation to finite-amplitude perturbations. *J. Phys. Oceanogr.,* **34,** 2305–2315.

Mysak, L. A., T. F. Stocker, and F. Huang, 1993: Century-scale variability in a randomly forced, two-dimensional thermohaline ocean circulation model. *Climate Dyn.,* **8,** 103–106.

Sévellec, F., T. Huck, and M. Ben Jelloul, 2006: On the mechanism of centennial thermohaline oscillations. *J. Mar. Res.,* **64,** 355–392.

Sirkes, Z., and E. Tziperman, 2001: Identifying a damped oscillatory thermohaline mode in a general circulation model using an adjoint model. *J. Phys. Oceanogr.,* **31,** 2297–2305.

Stommel, H., 1961: Thermohaline convection with stable regimes flow. *Tellus,* **13,** 224–230.

Sun, L., M. Mu, D.-J. Sun, and X.-Y. Yin, 2005: Passive mechanism of decadal variation of thermohaline circulation. *J. Geophys. Res.,* **110,** C07025, doi:10.1029/2005JC002897.

Tziperman, E., and P. J. Ioannou, 2002: Transient growth and

optimal excitation of thermohaline variability. *J. Phys. Oceanogr.,* **32,** 3427–3435.

——, J. R. Toggweiler, Y. Feliks, and K. Bryan, 1994: Instability of the thermohaline circulation with respect to mixed boundary conditions: Is it really a problem for realistic models? *J. Phys. Oceanogr.,* **24,** 217–232.

Wright, D. G., and T. F. Stocker, 1991: A zonally averaged ocean model for thermohaline circulation. Part I: Model development and flow dynamics. *J. Phys. Oceanogr.,* **21,** 1713–1724.

——, C. B. Vreugdenhil, and T. M. Hughes, 1995: Vorticity dynamics and zonally averaged ocean circulation models. *J. Phys. Oceanogr.,* **25,** 2141–2154.

——, T. F. Stocker, and D. Mercer, 1998: Closures used in zonally averaged ocean models. *J. Phys. Oceanogr.,* **28,** 791–804.

Zanna, L., and E. Tziperman, 2005: Nonnormal amplification of the thermohaline circulation. *J. Phys. Oceanogr.,* **35,** 1593–1605.

Zhang, S., C. A. Lin, and R. J. Greatbatch, 1992: A thermocline model for ocean-climate studies. *J. Mar. Res.,* **50,** 99–124.